Available online at www.sciencedirect.com

ScienceDirect

Energy Procedia 63 (2014) 5671 – 5679

Energy Procedia

GHGT-12

Geomechanical Behavior of Caprock and Cement: Plasticity in Hydrodynamic Seals

J. William Carey[a]*, Hiroko Mori[a], Diana Brown[a], and Rajesh Pawar[a]

Earth & Environmental Sciences Division, Los Alamos National Laboratory, Los Alamos, NM 87505 USA

Abstract

The geomechanical behavior of caprock and wellbore systems determines the robustness of the CO_2 storage system to disturbances from stress, pressure and temperature. In this study, we conduct triaxial coreflood and x-ray tomography experiments to directly measure permeability of water and supercritical CO_2 in caprock (shale and anhydrite), cement and synthetic wellbores. The observed plastic behavior and large deformation that occurred prior to distinct sample failure demonstrates substantial stress accommodation in these systems. Fracture development resulted in total sample permeability ranging from 10-1000 mD depending on sample properties and the applied stress configuration.

© 2014 The Authors. Published by Elsevier Ltd. This is an open access article under the CC BY-NC-ND license (http://creativecommons.org/licenses/by-nc-nd/3.0/).

Peer-review under responsibility of the Organizing Committee of GHGT-12

Keywords: CO_2 CO_2 sequestration; fracture permeability; triaxial experiments; x-ray tomography; wellbore integrity

1. Introduction

The buoyancy of supercritical CO_2 requires that caprock and wellbore systems provide a hydrodynamic seal that prevents upward migration of CO_2 to the surface or to underground drinking water sources. The geomechanical behavior of caprock and wellbore systems determines the robustness of the CO_2 storage system in response to stress, pressure and temperature (e.g., [1]). Injection of CO_2 will result in thermal- and pressure-generated stresses in the injection wellbore, in the storage reservoir, and at the caprock-reservoir interface that have the potential to compromise the integrity of the storage reservoir. In particular, recent concerns have focused on the potential of injection-triggered seismicity to damage the caprock seal [2].

* Correspoding author. Tel.: 1-505-660-8894
E-mail address: bcarey@lanl.gov

1876-6102 © 2014 The Authors. Published by Elsevier Ltd. This is an open access article under the CC BY-NC-ND license (http://creativecommons.org/licenses/by-nc-nd/3.0/).
Peer-review under responsibility of the Organizing Committee of GHGT-12
doi:10.1016/j.egypro.2014.11.600

In this study, we focus on the hydrologic consequences of geomechanical damage to caprock and wellbore systems. There are few experimental or field data available that provide measures of the effective permeability of damaged rock or cement. Typical caprock (e.g., shale or evaporite) and cement are not especially brittle materials and their capacity to support large fracture apertures with high permeability is unclear. In fact, the practice of using proppants in the hydraulic fracturing industry demonstrates the potential for limited as well as short-term transmissivity of fractured shale. These considerations emphasize the need to quantitatively evaluate fracture permeability in caprock and cement systems.

In this study, we present triaxial coreflood experiments to directly measure permeability of water and supercritical CO_2 in caprock and cement. We study the behavior of Utica shale (Pennsylvania and Ohio), anhydrite (Springerville, Arizona), Portland cement, and shale-cement-steel composites ("synthetic wellbore systems").

2. Methods

Experiments were conducted in a triaxial coreflood device that permits simultaneous application of independent confining and pore pressure to 35 MPa and axial load to 480 MPa. All fluids were delivered with Isco pumps and pore pressure was controlled using a backpressure regulator. Steady-state permeability measurements were conducted at constant flow-rate with pressure determined by inlet and outlet pressure transducers, although permeability was monitored continuously during sample deformation. The volumetric flow of CO_2 was measured with a wet gas meter in combination with an equation of state for CO_2. Sample deformation (strain) was measured using a combination of strain gages affixed directly to the samples and a linear variable displacement transducer (LVDT) that measured piston displacement. The axial load was calculated from the applied hydraulic oil pressure. We used x-ray tomography to characterize initial sample heterogeneity and subsequent fracture geometry with a resolution of 25 μm.

The experiments were conducted on 25 x 25 mm to 25 x 60 mm cylindrical samples at 20-45 ^{o}C with a relatively low confining pressure between 2 and 20 MPa. In the experiments, undamaged, impermeable samples were subjected to an increasing axial load until a discrete failure event was observed (generally as a rapid change in axial load pressure and/or change in the LVDT position). The samples were loaded in either a traditional compression configuration (flat, parallel anvils) or in a "pure shear" configuration using split anvils that generated a simple plane of shear stress. After sample failure, the axial load was returned to hydrostatic conditions for additional permeability characterization and observations of sample creep.

3. Results

3.1. Anhydrite

Fracture-permeability behavior of anhydrite (Springerville, AZ) was studied in compression at 45 ^{o}C and 11.7 MPa confining pressure with supercritical CO_2 as the pore fluid. As shown in Fig. 1, the initial stages of the experiment involved bringing the sample to hydrostatic conditions (11.7 MPa) in a series of steps. During this period, the LVDT recorded apparent shortening of the sample (about 1.8%) that reflects final seating of the rock core against the piston anvils. Permeability measurements of supercritical CO_2 at hydrostatic conditions were near 15 μD. It is likely that this permeability reflected some bypass of the core as we expected sub-μD permeability for this sample. At about 39,000 s, the axial load was steadily increased until sample failure occurred close to 120 MPa with a net deformation of about 0.91%. This sample was significantly stronger than other anhydrite rock core that failed at values closer to 50 MPa.

At the point of failure the sample shortened markedly (almost 2%) and the axial load fell to 50 MPa.

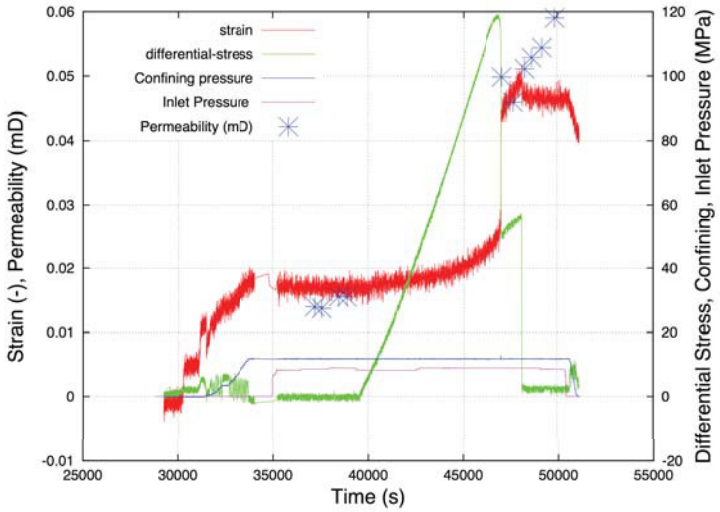

Figure 1. Experimental data for Springerville anhydrite showing LVDT-measured strain and permeability on the left axis and applied stress, confining pressure, and inlet pressure on the right axis all as a function of time.

We continued to apply an axial load to the sample and recorded permeability values of supercritical CO_2 that had increased to 45 μD. After the sample was returned to hydrostatic conditions, additional permeability values were obtained that increased slightly to 60 μD.

Post-experiment study of the sample using x-ray tomography revealed a dominant shear fracture system extending across the corners of the sample (Fig. 2). Numerous fine fault-splays emerge from the main shear fracture. Several larger fractures at high angles to the main fracture also developed.

3.2. Shale

Fracture-permeability relations for Utica Shale were studied in both compression and pure shear. In Fig. 3, we show strain gage behavior and permeability measurements in a compression experiment at 45 ^{o}C and 11.7 MPa. The strain gage data allow an estimate of the elastic properties of the system and yield a Young's modulus of 39 GPa and a Poisson ratio of 0.36 (measured between 10 and 50 MPa by the secant method). At about 85 MPa, the sample reaches its maximum strength and fails. The sample was then quickly returned to hydrostatic conditions in about 100 seconds.

Permeability was monitored by application of 8.3 MPa of supercritical CO_2 on the face of the core. There was no fluid communication across the core (the outlet pressure was near 0) until the sample fractured at 85 MPa. Under hydrostatic conditions, the measured permeability values were low, between 50 and 60 μD (Fig. 3).

X-ray tomography data for the sample showed a corner-to-corner fracture system with two primary branches (Fig. 4). In the lower left part of the sample, a more complex, penetrating set of fractures and greater damage developed.

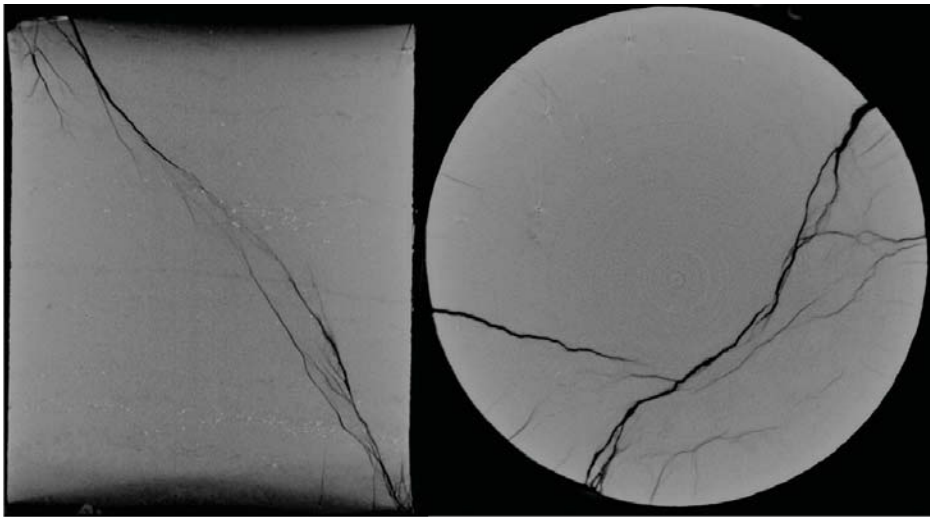

Figure 2. X-ray tomography of the Springerville anhydrite after the experiment showing the development of a shear fracture band and secondary fault spalys in a vertical slice (left) and horizontal slice (right).

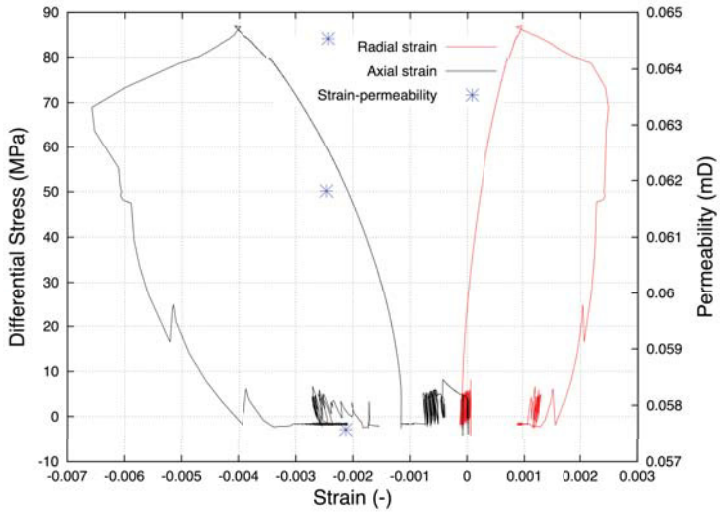

Figure 3. Experimental data for Utica Shale showing strain gage-measured strain versus axial load and permeability.

The strain recorded by the strain gages is typically smaller than that recorded by the LVDT (compare Figs. 1 and 3). This is because the LVDT measured total shortening of the rock core. In many cases, particularly after fracturing begins, deformation occurs in the system that is not observed by strain gages attached to one part of the rock core.

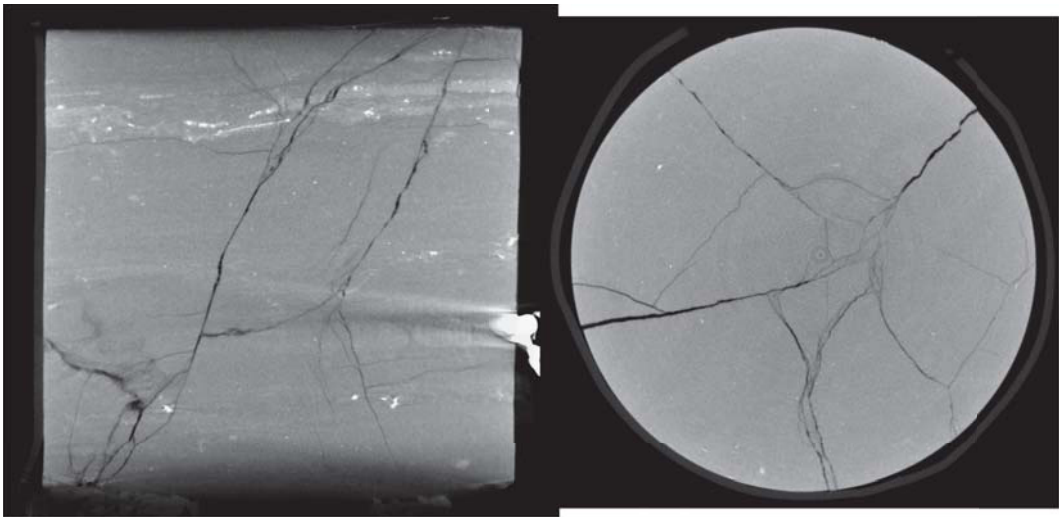

Figure 4. X-ray tomography data for Utica shale fractured in compression (vertical section on left; horizontal section on right).

3.3. Portland Cement

Fracture-permeability relations of Type G oilwell cement samples (water-cement ratio 0.4) were studied in both compression and pure shear. A compression experiment is shown in Fig. 5 that was conducted at 45 ^{o}C and 11.7 MPa confining pressure. The sample was first brought to hydrostatic conditions and then at about 34,000 s the differential stress was ramped upward to fracture the cement sample (Fig. 5).

At a net strain of about 1%, the sample began to deform plastically. At about 1.5% strain and 65 MPa differential stress, the cement started significant plastic deformation before achieving its ultimate strength of 78 MPa at about 5% strain. The experiment was ended at about 7% total strain.

The permeability of the cement was monitored by application of 8.2 MPa supercritical CO_2 on the face of the core (Fig. 5). Initially there was very little pressure communication but at a differential stress of 7 MPa the outlet pressure had increased to 6.0 MPa. However, further application of axial stress and sample deformation to 7% failed to result in any further increase in the outlet pressure. The sample remained impermeable throughout the experiment.

X-ray tomography showed that the cement sample had shortened and widened considerably due to 7% axial deformation (Fig. 6). However, fracture development was very limited without the formation of through-going fractures. This was consistent with the observed lack of permeability.

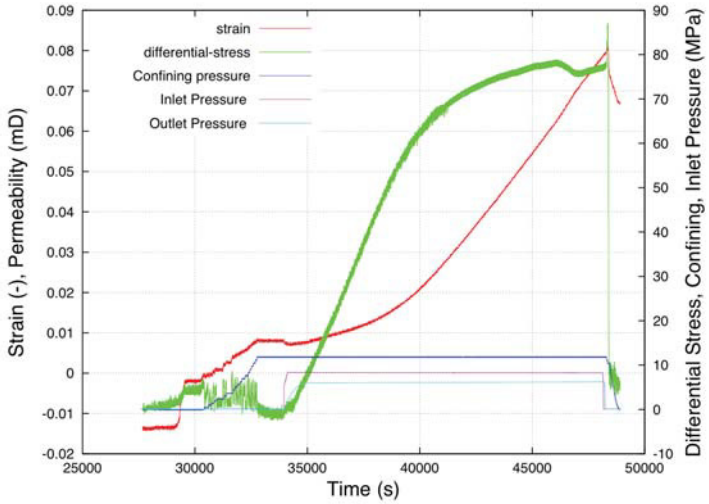

Figure 5. Experimental data for type G oilwell cement showing LVDT-measured strain on the left axis and applied stress, confining pressure, and inlet/outlet pressure on the right axis all as a function of time. The sample recorded no measureable permeability.

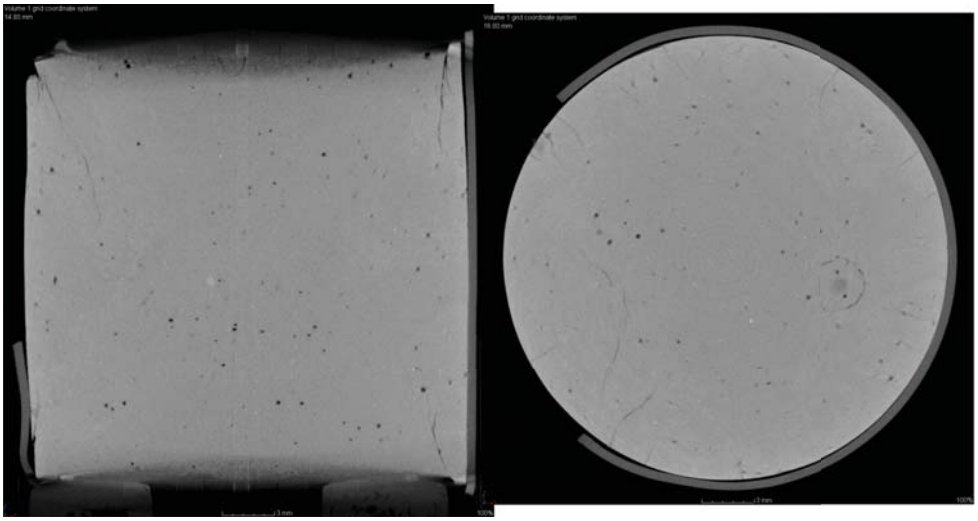

Figure 6. X-ray tomography images of type G oilwell cement (cf., Fig. 5) fractured in compression (vertical section on left; horizontal section on right).

3.4. Synthetic Wellbore Samples

In order to study the permeability behavior of interfaces in the wellbore system, a synthetic well was constructed of Utica shale, type G oilwell cement and a mild carbon steel rod. A 2.5-cm cylinder of shale was cored approximately in the center with a 1-cm bit. The central borehole was filled with type G oilwell cement and a 0.5-cm steel rod was embedded in the cement. Bedding in the shale was parallel to the axis of the borehole. The system represented a horizontal

well in a shale with horizontal bedding and included the shale-cement and steel-cement interfaces.

The experiments were conducted by placing the cylindrical specimen between the triaxial pistons and compressing the system at 45 ^{o}C and 20.7 MPa confining pressure (Fig. 7). A differential stress was applied to the synthetic wellbore system by reducing the confining pressure. The system showed no axial shortening until a differential stress in excess of 60 MPa was applied. This behavior is attributed to the presence of the steel rod with its large-magnitude Young's modulus. The sample also appeared to expand slightly as the confining pressure was reduced. The maximum strength of the system was achieved at 82 MPa (0.15% shortening), whereupon the composite began to deform plastically. The system continued to lose strength until a distinct fracture event at a shortening of 1.6%. At this point, the differential stress was removed and the sample was returned to hydrostatic conditions at 11.7 MPa.

During the experiment, permeability was monitored by application of 8.2 MPa of supercritical CO_2 against the inlet face of the core. No fluid communication was observed until a stress of 72 MPa was reached. Shortening at this point was minimal. Eventually sufficient deformation accumulated in the system for measureable permeability to develop that ranged from 0.4-0.6 mD while a differential stress was applied. Permeability reached almost 1 mD after the sample was returned to hydrostatic conditions (Fig 7.).

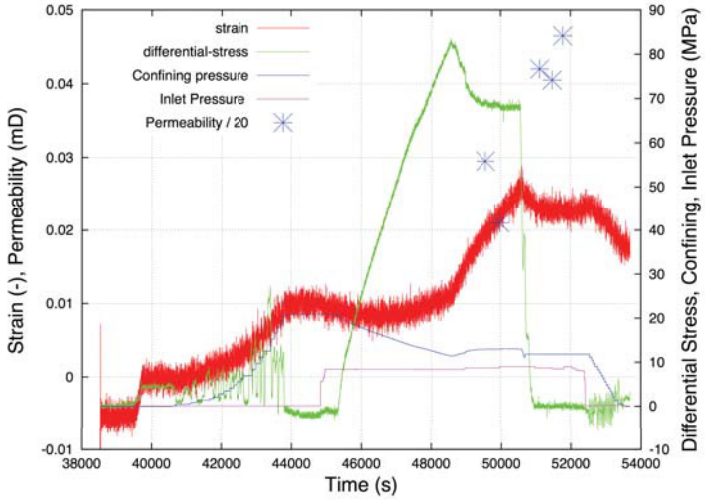

Figure 7. Experimental data for a synthetic well composite consisting of shale, type G oilwell cement and Steel. The data include the LVDT-measured strain and measured permeability (÷ 20) on the left axis and applied stress, confining pressure, and inlet pressure on the right axis all as a function of time. The sample recorded no measureable permeability.

X-ray tomography of the sample revealed that almost all of the inelastic deformation was accommodated by fracturing in the shale and separation at the shale-cement interface (Fig. 8). The shale fractured extensively along bedding planes. Some of these bedding-plane fractures connected with the shale-cement interface creating a hydrologic link between the shale matrix and the shale-cement annulus (horizontal section in Fig 8). The vertical cross-section showed that fractures in the shale also ran also connected along the length of the synthetic wellbore system. The oilwell cement appeared to be undamaged (no fractures) and the cement-casing interface was undisturbed.

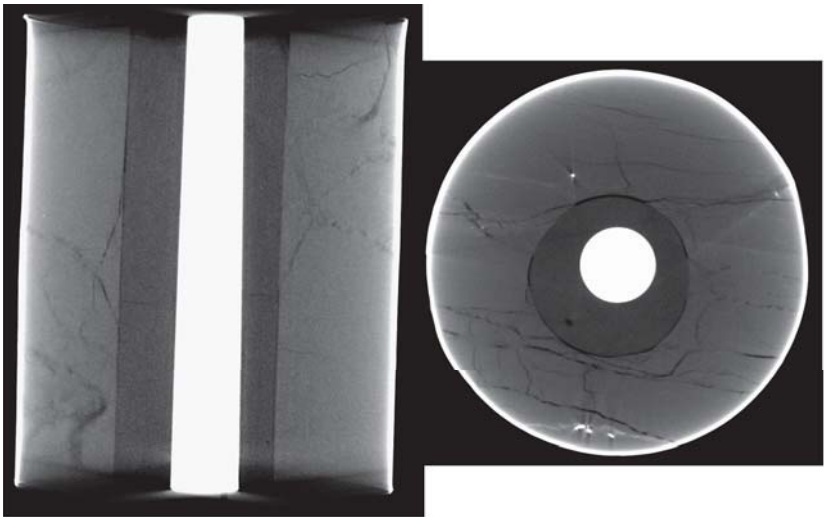

Figure 8. X-ray tomography images of a synthetic well fractured in compression consistsing of Utica shale on the outside, a central steel rod representing the casing in the center, and a filler of type G oilwell cement (cf., Fig. 7) (vertical section on left; horizontal section on right).

4. Conclusions

All of the materials (anhydrite, shale, Portland cement and wellbore composites) showed evidence of significant ductile behavior with distinct yield stresses followed by continued sample deformation. Anhydrite showed highly variable strength (a factor of 2) with the highest strength materials behaving in a distinctly brittle fashion. The oilwell cement samples reached their ultimate strength at 70-80 MPa and then either had a small fracture event followed by continuous deformation or simply plastically deformed until the end of the experiment. The shale samples generally had a period of plastic deformation after reaching their ultimate strength and then had a small, distinct fracture event. The shale then continued to plastically deform at reduced applied pressure until the end of the experiment.

Deformation in the synthetic wellbore systems was similar to that of shale but the interpretation is complicated by the heterogeneous composite of shale, oilwell cement and steel rod. In these systems, an ultimate strength was achieved and then a prolonged period of plastic deformation occurred prior to abrupt sample failure.

Fracture patterns differed among the materials. Anhydrite developed regular, high-angle fractures to the applied stress. These were simple in form. Shale fractures were complex and often dominated by adhesion between the piston faces and the samples (coning). The layering in shale produced more complex fracture patterns where they were perpendicular to the axial load. Portland cement fracture development was very limited and appeared in x-ray tomography to be the most plastic of the materials studied. In the synthetic wellbore samples, all of the fracture development occurred in the surrounding shale and at the shale-cement interface. The Portland cement did not show fracture evidence nor was there any separation at the cement-steel interface. However, the lack of deformation in the cement may have been due to the formation of a stress shadow around the steel casing.

Prior to deformation, the samples generally had no measurable permeability (<1 μD). In some cases, sample permeability increased very slightly with increasing deformation. In other cases, permeability did not increase until distinct fracture events. Sample deformation including fracturing led to modest increases in total sample permeability with maximum values on the

order of 10 mD in the compression experiments. The measured permeability decreased with increasing hydrostatic pressure. However, we note that the permeability of samples fractured in compression is limited by the connectivity of the resulting fracture system with the piston faces. Experiments in pure shear (not described in detail here) show much greater permeability to values as high as 1 D.

The observed plastic behavior and large deformation that occurred prior to distinct sample failure demonstrates substantial plastic behavior in these caprock, cement and wellbore systems. Depending on the state of stress (and amount of resulting strain), these systems may be able to incorporate substantial geomechanical damage without fracturing and without substantial permeability increases. Even where these systems fracture, the resulting permeability is limited. These experiments have been conducted at low effective confining pressure (12 MPa corresponds to about 600 m depth); higher confining pressures (and temperatures) will result in greater ductility and less tendency for damage-induced permeability enhancement.

Acknowledgements

The authors are grateful to the DOE-Fossil Energy program for support from FE-102-002-FY10 and FE-371-14-FY14. We thank Steve Chipera and Chesapeake Energy for providing shale samples and shale analyses. We thank Tim Ickes for the x-ray tomography analyses.

References

[1] Verdon, JP, Kendall, J-M., Stork, AL, Chadwick, RA, White, DJ, Bissell, RC Comparison of geomechanical deformation induced by megatonne-scale CO_2 storage at Sleipner, Weyburn, and In Salah. Proc Nat Acad Sci 2013; 110:E2762–E2771.

[2] Zoback, MD, Gorelick, SM Earthquake triggering and large-scale geologic storage of carbon dioxide. Proc Nat Acad Sci 2012; 109:10164–10168.